

Development of the radiation-hard MALTA CMOS sensor for tracking applications

G. Gustavino,^{a,*} P. Allport,^b I. Asensi Tortajada,^a P. Behera,^c D.V. Berlea,^d D. Bortoletto,^e C. Buttar,^f F. Dachs,^a V. Dao,^a G. Dash,^c D. Dobrijevic,^{a,h} L. Fasselt,^d L. Flores Sanz de Acedo,^a A. Gabrielli,^a M. Gaži,^e L. Gonella,^b V. González,^g P. Jana,^c L. Li,^b H. Pernegger,^a P. Riedler,^a W. Snoeys,^a C. A. Solans Sanchez,^a T. Suligoj,^h M. van Rijnbach,^{a,i} M. Vázquez Núñez,^{a,g} A. Vijay,^c J. Weick,^{a,j} S. Worm^d and A. M. Zoubir^j

^aCERN, Geneva, Switzerland

^bUniversity of Birmingham, Birmingham, United Kingdom

^cIndian Institute of Technology Madras, Chennai, India

^dDESY, Zeuthen, Germany

^eUniversity of Oxford, Oxford, United Kingdom

^fUniversity of Glasgow, Glasgow, United Kingdom

^gUniversity of València, València, Spain

^hUniversity of Zagreb, Zagreb, Croatia

ⁱUniversity of Oslo, Oslo, Norway

^jTechnische Universität Darmstadt, Darmstadt, Germany

E-mail: giuliano.gustavino@cern.ch

The MALTA family of Depleted Monolithic Active Pixel Sensors (DMAPS) is produced using Tower 180 nm CMOS technology, specifically targeting radiation-hard applications in the HL-LHC and beyond. Several process modifications have resulted in radiation hardness up to 3×10^{15} 1 MeV n_{eq}/cm^2 and time resolution below 2 ns, with uniform charge collection efficiency across the chip formed of 512×224 pixels with a size of $36.4 \times 36.4 \mu m^2$. This is achieved when adopting high-resistivity Czochralski substrates with backside metallisation to obtain a good propagation of the bias voltage. This contribution will show the most recent results obtained on MALTA2 chip demonstrators, including signal efficiency, noise occupancy and time resolution, at different levels of irradiation as well as the performance of the MALTA telescope permanently installed at the SPS at CERN and used in the test beam campaign in 2021-2023.

The 32nd International Workshop on Vertex Detectors (VERTEX2023)

16-20 October 2023

Sestri Levante, Genova, Italy

*Speaker

1. Introduction

High-energy physics experiments require an unprecedented level of precision for detecting extremely rare events within dense experimental environments. Monolithic pixel technologies provide several advantages with respect to the more often adopted hybrid silicon pixel sensors for detectors at colliders. They allow to minimise the material budget, the power consumption and reduce construction costs by exploiting the industrial CMOS production process of commercial foundries. Then, the read-out electronics are integrated into the same silicon wafer of the sensor, avoiding the need for custom expensive bump-bonding. Additionally, pixel designs with small collection electrodes reduce the sensor capacitances hence increasing the signal-over-noise ratio even with a limited thickness of the active layer. These characteristics made them suitable for large surface detectors such as the ALICE Inner Tracking System [1] installed during the second long shut-down of LHC. However, their tolerance to extreme radiation fluences is today a critical area of investigation. The MALTA project focuses on developing a chip based on radiation hard Depleted Monolithic Active Pixel Sensor (DMAPS) which fulfils the requirements of the future collider experiments.

2. MALTA2

The MALTA2 chip is the second generation of the full-scale prototypes produced in the MALTA family. It incorporates a matrix of 512×224 pixels within a total surface area of $18 \times 9 \text{ mm}^2$. The sensor is a DMAPS prototype developed in the Tower Semiconductor 180 nm CMOS imaging process, modified with an additional low dose n-type implant. The pixel size is $36.4 \times 36.4 \text{ }\mu\text{m}^2$ with a thickness of 50, 100 or 300 μm . The sensors are produced with two different kinds: high-resistivity p-type epitaxial layer (Epi) and high-resistivity p-type Czochralski (Cz) substrate. The latter is operational up to higher substrate voltage, resulting in larger depleted regions yielding higher radiation resistance and cluster size [2]. To increase the lateral electric field in the pixel corners two additional process modifications have been produced: a gap in the low dose n-type implant (NGAP) or an additional p-type implant at the pixel border (XDPW). They provide similar performance resulting in a relatively shorter collection time and higher efficiency than the standard process [3]. A small octagonal-shaped collection electrode with a 2 μm diameter guarantees a minimal capacitance (5 fF) implying a low power consumption (10 mW/cm² digital at 100 MHz/cm² and 70 mW/cm² analog power). The main difference from the first generation of the MALTA chip prototype lies in the front-end [4, 5]. It involves the addition of a cascoded stage in the input branch and the use of larger transistors in the amplifier's feedback loop. This results in reduced noise and improved gain, enabling the chip to operate with thresholds down to $\mathcal{O}(100) e^-$. The chip employs an asynchronous read-out design that avoids the need to propagate a clock signal throughout the pixel matrix, thus reducing digital power consumption. When a particle traverses the sensor, the in-pixel digital circuitry transmits the hit information from the chip to the periphery using a sequence of short pulses corresponding to the pixel's address. Pixels are organised in a dedicated group logic allowing to operate at hit rates well above 100 MHz/cm². A backside metallisation process is performed to achieve a uniform propagation of the substrate voltage across the whole chip.

3. The MALTA telescope

A successful application of the MALTA chips is a six-tracking planes telescope permanently installed at SPS at CERN [6]. It can additionally host two Devices Under Test (DUTs) simultaneously that can be located inside a cold box to maintain a dry and low-temperature environment suitable for irradiated chips. The cold-box is positioned between the innermost telescope planes both operated with a 30 V reverse substrate bias enhancing the cluster size. A scintillator is placed behind the six planes to provide a precise timing reference. The trigger system of the telescope is fully configurable, enabling triggering on coincidence between the telescope planes and the scintillator. The spatial resolution of the MALTA telescope was measured as a function of the number of planes considered in the track reconstruction as shown in Figure 1. The results obtained by performing linear fits and extracting the uncertainty of the intercept on the most upstream DUT are compared with the analytical estimation that relies on the telescope geometry. The full telescope spatial resolution is $\sigma_s = 4.1 \pm 0.2 \mu\text{m}$. A clear gain in terms of spatial resolution is provided by the larger cluster size of the innermost planes. Assuming a uniform response of the DUT along the pixel pitch, the resolution is alternatively estimated from the fit of the convolution of a Gaussian with a two-sided step function on the distribution of the tracks' residuals on a DUT. The resulting width extracted from the Gaussian fit is $\sigma_s = 4.7 \pm 0.2 \mu\text{m}$. The effects of inhomogeneity and time resolution at the DUT edges contribute to inflating the overall resolution estimation providing a larger value if compared with both the analytical description and the linear regression measurement.

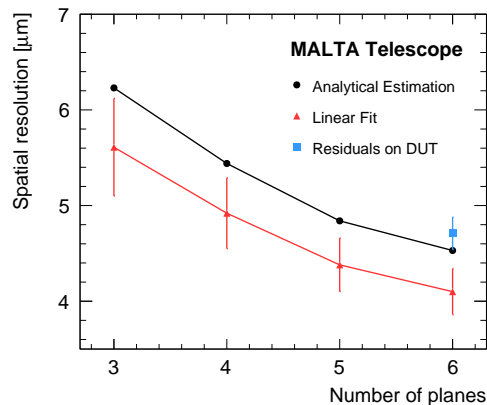


Figure 1: Telescope resolution as a function of the number of planes considered. Black: analytical estimation. Red: measurements based on the linear fits. Blue: estimation based on the fit of the convolution of a Gaussian with a two-sided step function on the distribution of the residuals on a DUT.

4. MALTA2 performance

A campaign of test beam measurements has been performed between 2021 and 2023 at SPS at CERN exploiting the 180 GeV proton beamline and the MALTA telescope to evaluate the radiation tolerance of the MALTA2 chips. The following results resume the findings of a rich characterisation and include the performance of the samples based on the most promising Cz substrate with the aforementioned process modifications [7].

4.1 Efficiency and cluster size

MALTA2 samples are fully efficient over the entire matrix when un-irradiated at the reverse substrate bias of 6 V. The average cluster size achieved is about 2 at operational thresholds of $\mathcal{O}(100)e^-$. After neutron irradiation, the effect of charge trapping can be mitigated by increasing the substrate voltage, hence extending the drift volume in the sensor. The average chip efficiency as a function of the reverse substrate bias is shown in Figure 2a for different irradiation doses at similar threshold configurations. An efficiency greater than 95% is observed for fluences of 2×10^{15} 1 MeV n_{eq}/cm^2 at reverse bias voltages greater than about 20 V. Similarly, a larger average cluster size can be achieved by increasing the substrate voltage to mitigate the charge trapping effect and to increase the active depths enhancing the charge sharing effect between pixels. The efficiency loss at higher irradiation doses is found to originate from the pixel corners. Here, the radiation damage impacts the electric field degrading the charge collection efficiency. To tackle this effect, a higher doping concentration of the n-layer can better compensate for the possible type inversion at elevated fluence levels and maintain a sufficient separation from the p-type substrate. A comparison between the average efficiency of the chips with the two different doping concentrations of the n-layer at the radiation of 3×10^{15} 1 MeV n_{eq}/cm^2 is shown in Figure 2b. While for lower doping only an efficiency of about 90% can be achieved, a full efficiency in the very-high doping configuration is obtained at substrate voltages higher than about 30 V and an average cluster size up to 1.7 pixels at 55 V.

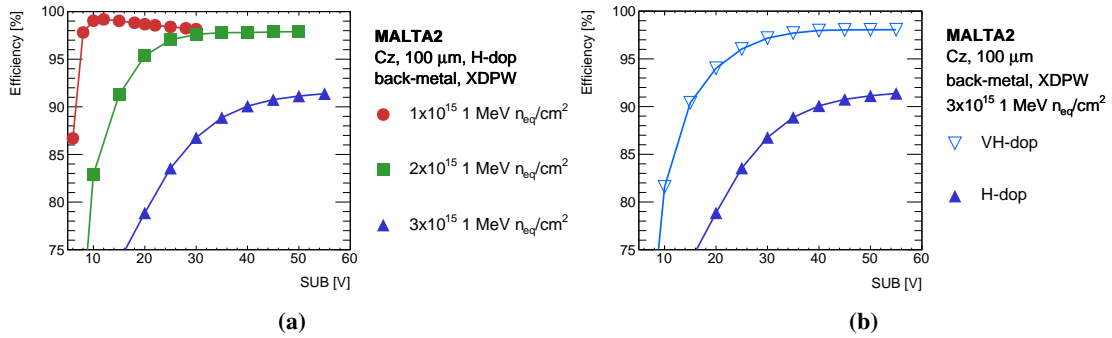


Figure 2: Figure 2a: average efficiency versus bias voltage for MALTA2 samples irradiated to 1, 2, and 3×10^{15} 1 MeV n_{eq}/cm^2 . The results are shown at the operating threshold with the highest efficiency, corresponding to 240, 260, and 120 e^- , respectively. Figure 2b: comparison of the average efficiency versus bias voltage of MALTA2 chips with a high (H-dop) and very-high doping concentration (VH-dop) of the n-layer at the radiation of 3×10^{15} 1 MeV n_{eq}/cm^2 . The latter chip is shown at the operating threshold with the highest efficiency, corresponding to 110 e^- .

Operating windows with an efficiency $>95\%$ and noise occupancy lower than 40 Hz can be defined for the irradiated samples at 3×10^{15} 1 MeV n_{eq}/cm^2 for different threshold configurations. These requirements are chosen to comply with the ATLAS ITk requirements. In Figure 3a a comparison of a sample with a regular backside and one with the back metallisation is provided at the same substrate voltage. Even by applying a fiducial selection on the former chip to guarantee a good propagation of the reverse bias voltage, there is a clear gain in performance derived from the back-metallisation process. Further, the operating windows of the back metallised sample for

different substrate voltages are compared in Figure 3b. All the setups demonstrate that the noise criteria are met and the operating windows are just defined by the efficiency requirements.

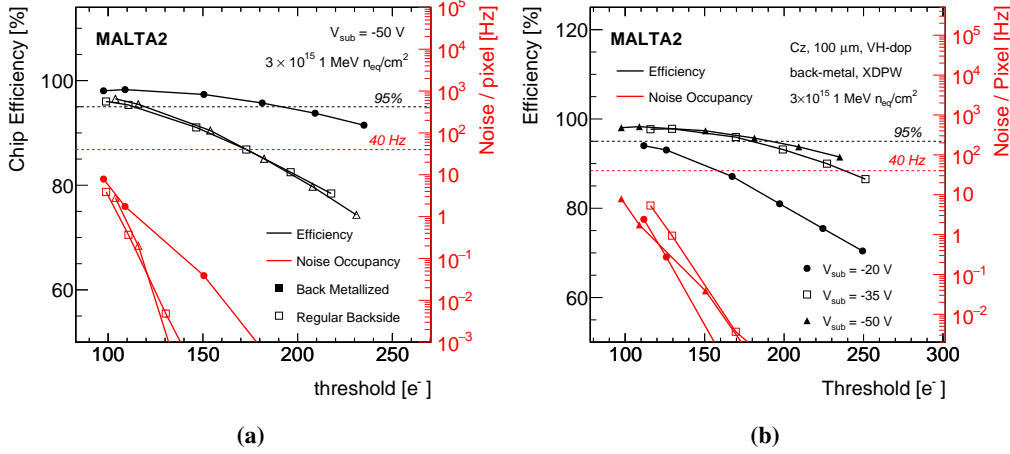


Figure 3: Average efficiency (in black) and noise occupancy (in red) as a function of threshold in electrons of MALTA2 samples irradiated to 3×10^{15} 1 MeV n_{eq}/cm² with very-high doping of the n-layer. In Figure 3a the performance of a backside metallisation sample is compared with one with a regular backside. Only about 5% of the latter sample is considered by applying a fiducial selection to guarantee a good propagation of the bias voltage. In Figure 3b the performance of the back-metallised sample is shown at the reverse substrate voltages of 20, 35, 50 V.

4.2 Timing

The timing performance is evaluated by measuring the time of arrival of the fastest hit in a pixel cluster with respect to the scintillator reference. A correction that takes into account the time propagation of the hit information due to the structure of the chip read-out is applied. For un-irradiated chips, the measured time resolution of $\sigma_t = 1.7$ ns is obtained from the width of a Gaussian fit of the core of the time difference distribution. This includes both sensor intrinsic effects due to the time-walk, charge collection, electronics jitter and external effects such as the jitter of the trigger scintillator (of about 0.5 ns) and the FPGA sampling jitters (of about 0.9 ns). The in-time efficiency, obtained by integrating the time of arrival distributions in different time ranges, is found to be greater than 98% for a 25 ns time window, suitable for applications at the LHC. With the increase of irradiation doses, the uniformity of the time response degrades due to the charge trapping effect and because of the mobility change of the charge carriers. Figure 4a shows the variation of the timing resolutions for different fluence levels as a function of the substrate voltage. In the case of irradiated chips, the root-mean-square (RMS) of the time difference distributions is used given the more prominent tails. It is evident how the uniformity of the mean time of arrival of the leading hit deteriorates as the radiation dose increases. However, as in the case of the efficiencies, enhancing the reverse bias voltages improves the timing performance. Figure 4b shows the relative shift of the mean time of a hit as a function of the associated telescope track distance from the pixel centre. Further investigations based on simulations are needed to describe the source of this behaviour. Studies to estimate the depletion depth of the tested pixels are also ongoing. The increased doping

concentration of the n-layer mitigates the effects of the irradiation where about 95% of the hits are collected within 25 ns at a fluence of 3×10^{15} 1 MeV $n_{\text{eq}}/\text{cm}^2$.

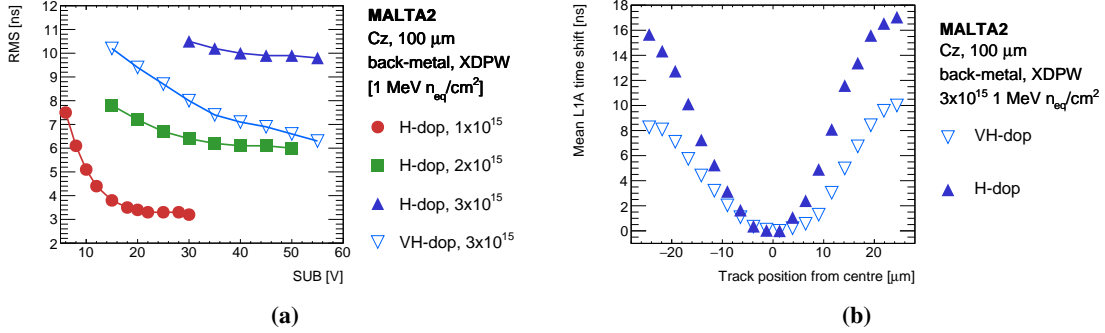


Figure 4: Figure 4a: RMS of the timing difference distribution as a function of the substrate voltage. Only data points where the detection efficiency lies above 85% are considered. Three samples with high doping of the n-layer are irradiated to 1, 2, and 3×10^{15} 1 MeV $n_{\text{eq}}/\text{cm}^2$ and operated at the threshold with the highest efficiency, corresponding to 240, 260, and 120 e-, respectively. A sample irradiated to 3×10^{15} 1 MeV $n_{\text{eq}}/\text{cm}^2$ features the very-high doping of the n-layer and it is operated at the threshold with the highest efficiency, corresponding to 110 e-. Figure 4b: relative shift of the mean time of arrival of the leading hit within a cluster with respect to a scintillator reference, as a function of the distance of the associated telescope track from the pixel centre. The samples are both operated at the reverse bias voltage of 55 V and differ in the doping level of the n-layer.

5. Conclusions

MALTA2 is the latest full-scale DMAPS prototype of the MALTA project. The first successful application of the MALTA chips is a telescope composed of six planes with a resulting spatial resolution $\sigma_s = 4.1 \pm 0.2 \mu\text{m}$ and a timing resolution of $\sigma_t = 2.1$ ns. It has been permanently installed at SPS at CERN since 2021 and is currently used to study the performance of the new generation of MALTA chips and other ATLAS upgrade projects. A large set of characterisation studies has been performed in the test beam campaign between 2021 and 2023. They demonstrate how the combination of pixel design, process and design modifications, using the high-resistivity Cz substrates with backside metallisation implemented in the MALTA2 chips can fulfil the requirements of the future LHC experiments up to irradiation doses of 3×10^{15} 1 MeV $n_{\text{eq}}/\text{cm}^2$. At this fluence level, samples with a higher doping concentration in the n-layers can reach up to 98% efficiency and an average cluster size of 1.7 pixels when operated at a threshold of 110 e- and a reverse bias voltage of 55 V. In this configuration, 95% of the clusters are collected within 25 ns. A more precise and uniform timing response across the pixels is obtained when compared to a sample with a lower n-layer doping irradiated at the same fluence.

Acknowledgments

This project has received funding from the European Union's Horizon 2020 Research and Innovation programme under Grant Agreement numbers 101004761 (AIDAInnova), 675587 (STREAM),

and 654168 (IJS, Ljubljana, Slovenia).

References

- [1] ALICE Collaboration, “Technical Design Report for the Upgrade of the ALICE Inner Tracking System”, *J. Phys. G* **41** (2014), 087002.
- [2] H. Pernegger *et al.* “MALTA-Cz: a radiation hard full-size monolithic CMOS sensor with small electrodes on high-resistivity Czochralski substrate”, *JINST* **18** (2023) no.09, P09018.
- [3] M. Munker *et al.* “Simulations of CMOS pixel sensors with a small collection electrode, improved for a faster charge collection and increased radiation tolerance”, *JINST* **14** (2019) no.05, C05013.
- [4] M. Dyndal *et al.*, “Mini-MALTA: Radiation hard pixel designs for small-electrode monolithic CMOS sensors for the High Luminosity LHC”, *JINST* **15** (2020) no.02, P02005.
- [5] F. Piro *et al.*, “A $1\mu\text{W}$ Radiation-Hard Front-End in a $0.18\text{-}\mu\text{m}$ CMOS Process for the MALTA2 Monolithic Sensor”, *IEEE Trans. Nucl. Sci.* **69** (2022) no.6, 1299-1309.
- [6] M. van Rijnbach *et al.*, “Performance of the MALTA telescope”, *Eur. Phys. J. C* **83** (2023) no.7, 581.
- [7] M. van Rijnbach *et al.*, “Radiation Hardness of MALTA2 Monolithic CMOS Sensors on Czochralski Substrates”, arXiv:2308.13231.